Nanotubes

DOI: 10.1002/ange.200502870

Hollow and Polygonous Microtubes of Monocrystalline Indium Germanate

Jinhua Zhan, Yoshio Bando, Junqing Hu, Longwei Yin, Xiaoli Yuan, Takashi Sekiguchi, and Dmitri Golberg*

Since the identification of carbon nanotubes in 1991,[1] a challenging research field has been launched in materials science, solid-state physics, and chemistry, ensuring a wide range of exciting practical applications. Over the last decades there has been a continuous interest in exploring layered or nonlayered materials that form tubular structures. Generally, the generation of inorganic tubular forms has been based on layered binary inorganic compounds, such as BN, MoS_2, WS_2, VS_2, GaS, VO_x, TiO_2 etc.[2] The tubular forms of elemental or binary inorganic compounds with 3D nonlayered crystal structures have usually been fabricated by using carbon nanotubes, porous membranes, or removable nanowires as templates[3] to give amorphous or polycrystalline nanotubes. Single-crystalline tubes have occasionally been generated based on epitaxial casting. Germanates have attracted attention as important catalyst materials, scintillators for detection of low-energy solar neutrinos in agreement with Raghavan's nuclear reaction, and porous ceramic materials for humidity sensors.[4] Indium germanate ($In_2Ge_2O_7$) has a specific laminar thortveitite-type ($Sc_2Si_2O_7$) structure.[5] Herein, we demonstrate the successful synthesis of ternary indium germanate tubes with sub-micrometer diameters and present a thorough analysis of their morphological and structural characteristics.

Carbon-assisted thermal evaporation of an In_2O_3/GeO_2 powder mixture under a stream of Ar in a horizontal resistance furnace results in the formation of a white product on the inner wall of the tube (downstream), where the temperature is around 600 °C during heating. As shown in the scanning electron microscopy (SEM) image (Figure 1 a), the product is composed of numerous whiskers whose length reaches hundreds of micrometers. High-magnification SEM images (Figure 1 b) reveal that these whiskers have open tips and display tubular geometries. The cylinder pores of the tubular whiskers are either hexagonal or round. The powder X-ray diffraction (XRD) pattern of the product (Figure 1 c) suggests that it is composed of pure monoclinic $In_2Ge_2O_7$ (JCPDS card 26-0768: $a = 6.658$, $b = 8.784$, $c = 4.927$ Å, $\beta = 102.48°$; space group: $C2/m$). No characteristic peaks from other impurities, such as In_2O_3, GeO_2, In, or Ge, are detected in the XRD pattern.

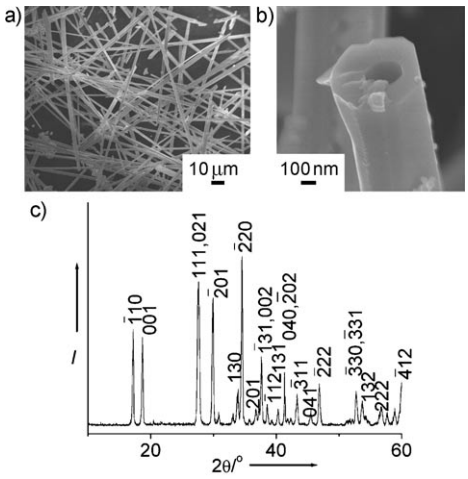

Figure 1. a) SEM image of $In_2Ge_2O_7$ tubes; b) high-magnification SEM image of a single tube revealing the open tip; c) XRD pattern of the product.

Detailed structural and chemical analyses of the products were carried out by TEM, high-resolution TEM, electron diffraction (ED), and energy-dispersive X-ray spectroscopy (EDS). Figure 2 shows a TEM micrograph of a typical $In_2Ge_2O_7$ tube. The diameter of this tube is about 600 nm and its cavity width is about 200 nm. Energy-dispersive X-ray spectra generated with an electron nanoprobe (diameter of around 50 nm) were collected from various regions of the

[*] Dr. J. Zhan, Prof. Y. Bando, Dr. L. Yin, Prof. D. Golberg
Advanced Materials Laboratory
National Institute for Materials Science (NIMS)
Namiki 1-1, Tsukuba, Ibaraki 305-0044 (Japan)
Fax: (+81) 29-851-6280
E-mail: ZHAN.Jinhua@nims.go.jp
Dr. J. Hu
International Center for Young Scientists (ICYS), NIMS
Namiki 1-1, Tsukuba, Ibaraki 305-0044 (Japan)
Dr. X. Yuan, Prof. T. Sekiguchi
Nanomaterials Laboratory, NIMS
Namiki 1-1, Tsukuba, Ibaraki 305-0044 (Japan)

Supporting information for this article is available on the WWW under http://www.angewandte.org or from the author.

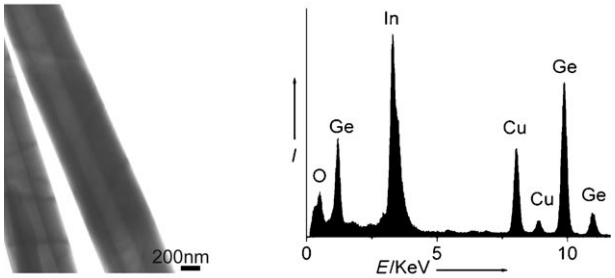

Figure 2. Typical TEM image of hollow $In_2Ge_2O_7$ microtubes (left) and a representative EDS spectrum (right) of a hollow $In_2Ge_2O_7$ microtube.

$In_2Ge_2O_7$ tube. They verify the uniformity of the indium and germanium compositions—the overall ratio of indium to germanium is close to 1:1. A typical EDS spectrum is shown in Figure 2.

Figure 3a clearly demonstrates that the tip of the $In_2Ge_2O_7$ tube is open. The corresponding selected-area electron diffraction (SAED) pattern is depicted in Figure 3b. This pattern can be indexed as that recorded along the [$\bar{1}$10] zone axis of a monoclinic $In_2Ge_2O_7$ crystal. Electron diffraction (ED) patterns taken from various domains of the tube were strikingly similar, which clearly suggests its single-crystalline nature. Other $In_2Ge_2O_7$ tubes were also confirmed to be perfect single crystals. Streaking of the reflections in the

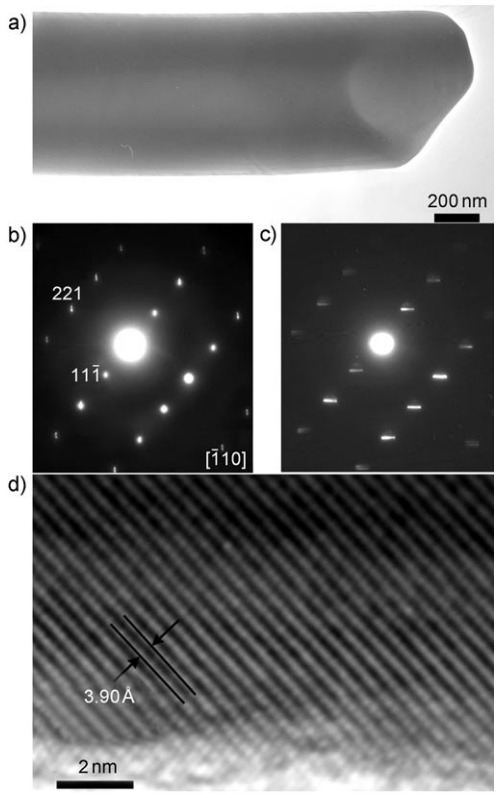

Figure 3. a) TEM image of an isolated open-ended hollow $In_2Ge_2O_7$ microtube; b) SAED pattern of a hollow $In_2Ge_2O_7$ microtube recorded along the [$\bar{1}$10] zone axis, and c) its corresponding underfocused SAED pattern; d) a high-resolution TEM image of the hollow $In_2Ge_2O_7$ microtube along the [$\bar{1}$10] direction.

underfocused electron diffraction pattern (Figure 3c) implies that the preferred tube growth direction is parallel to the (003) plane. High-resolution TEM images additionally reveal that the as-obtained $In_2Ge_2O_7$ tubes are structurally uniform single crystals. An HRTEM image taken at the edge of a $In_2Ge_2O_7$ tube (Figure 3d), shows clearly resolved fringes separated by 3.90 and 2.15 Å, which correspond to the (221) and (11$\bar{1}$) lattice spacings of a monoclinic $In_2Ge_2O_7$ crystal, respectively.

Another SAED pattern (Figure 4a), obtained after the $In_2Ge_2O_7$ tube was tilted inside the TEM, is shown in Figure 3a. The latter agrees well with the [110] zone axis of monoclinic $In_2Ge_2O_7$. As before, streaking of the reflections

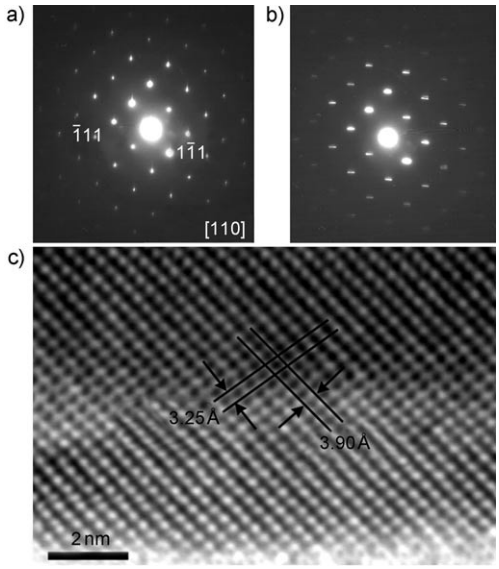

Figure 4. a) SAED pattern of a hollow $In_2Ge_2O_7$ microtube recorded along the [110] zone axis, and b) its corresponding underfocused SAED pattern, which reveals that the preferential growth direction is nearly parallel to the (002) plane; c) a high-resolution TEM image of the microtube wall along the [110] direction ($d_{\bar{1}11} = 3.90$ Å; $d_{1\bar{1}1} = 3.25$ Å, as marked by double lines).

in the underfocused ED pattern (Figure 4b) implies that the preferred growth direction is parallel to the (002) plane. Figure 4c depicts the HRTEM image corresponding to the [110] zone axis. The lattice fringes of the ($\bar{1}$11) and (1$\bar{1}$1) planes, with a d spacing of 3.90 and 3.25 Å, respectively, can be clearly seen. This indicates that the (002) plane is parallel to the edge of the $In_2Ge_2O_7$ tube. As seen from these images, this tube is a structurally uniform single crystal, the tube edge is clean, and there is no amorphous layer covering the surface. Upon taking the ED patterns and HRTEM images into account, one can suggest that the preferred growth direction of the tube is close to the [100] axis of the $In_2Ge_2O_7$ crystal.

Apart from the anisotropic growth of inorganic compounds in a solution modified by specific molecules,[6] anisotropic growth in the vapor phase generally results from the vapor–solid (VS) or vapor–liquid–solid (VLS) growth mechanisms.[7,8] The key feature of the VLS growth mechanism is that one end of a 1D nanostructure is capped with an alloy droplet. During the VLS growth process, this metal

particle may act as a preferential site for the absorption of incoming vapors to form a liquid alloy. Once the absorbed reactant is supersaturated within the liquid alloy droplet at a given temperature, it nucleates. Further condensation of the reactant vapors results in the continuous axial growth of a 1D structure. In contrast, the anisotropic growth during the VS growth process might be controlled by some kinetic and intrinsic crystallographic properties. Temperature and supersaturation are therefore the two dominant factors affecting the morphology of the products during the VS growth process.

As there are no metal-containing caps at the single-crystalline $In_2Ge_2O_7$ tubes, it is assumed that a VS growth process lies behind the present growth. During the synthesis, In_2O_3 and GeO_2 can react with the carbon powder to produce gaseous In_2O and GeO. From a thermodynamic point of view, the equilibrium pressures of gaseous In_2O and GeO at 1000 °C are similar to each other and reach over 100 kPa. In_2O and GeO, which are brought by the Ar flow to the lower-temperature furnace zone ($\approx$600 °C), can recombine with the residual oxygen in the furnace to form $In_2Ge_2O_7$—a stable ternary oxide of indium and germanium at ambient pressure.[9] Figure 5 displays a schematic illustration of a mono-

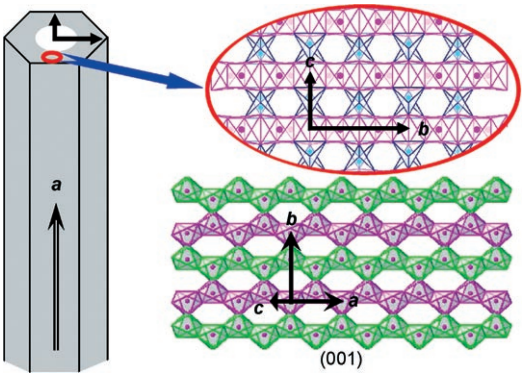

Figure 5. Network structure in of a hollow $In_2Ge_2O_7$ microtube.

crystalline $In_2Ge_2O_7$ tube. In the $In_2Ge_2O_7$ crystals, each In atom is coordinated to six O atoms to form an $\{InO_6\}$ octahedron. These $\{InO_6\}$ octahedra lie in a nearly hexagonal arrangement in the (001) plane and share edges to form a distorted honeycomb ensemble with the composition $\{[In_2O_6]^{6-}\}_n$. Each Ge atom is coordinated to four O atoms to form a tetrahedron. Two $\{GeO_4\}$ tetrahedra share one corner to form a $[Ge_2O_7]^{6-}$ group. The monoclinic $In_2Ge_2O_7$ lattice can therefore be described as a stacking of alternating parallel sheets of InO_6 octahedra and isolated $[Ge_2O_7]^{6-}$ groups (see Supporting Information). As demonstrated in the right-hand bottom panel of Figure 5, a honeycomb sheet of $\{InO_6\}$ octahedra can be viewed as a building block composed of edge-sharing, one-dimensional $\{In_nO_{4n+2}\}$ chains along the [100] axis. This anisotropic crystallographic feature may lead to the one-dimensional growth along the [100] axis. Analogous preferential growth patterns have also been frequently documented in some elemental or binary compounds composed of chain-like building blocks.[11–14] The formation of a specific tubular form may be attributed to several kinetic factors. When the evaporation temperature increases, the pores of tubular $In_2Ge_2O_7$ become larger. During the VS growth process, the interplay between the rates of deposition and surface diffusion becomes important. Generally, raising the temperature increases the growth rate exponentially according to the Arrhenius relation ($k = A\,e^{-Q/RT}$). At a higher growth temperature, the edge-growth rate prevails over the diffusion rate, giving rise to the growth of tubular $In_2Ge_2O_7$. An analogous growth mechanism has also been proposed for Sb_2S_3, AlN, GaN, InP, and MgO nanotubes.[14–18] It is notable that this growth scenario is quite different from that of layered compounds (such as C, BN, and MoS_2), which form nanotubes by molecular layer rolling.[1,2]

Finally, the optical properties of $In_2Ge_2O_7$ tubes were analyzed by means of high-spatial-resolution cathodoluminescence (CL) spectroscopy and imaging. To visualize the spatial distribution of the luminescence from a single $In_2Ge_2O_7$ tube, a CL image was recorded at room temperature and at a wavelength of 560 nm. Figure 6a shows the SEM image of an individual $In_2Ge_2O_7$ tube. Its corresponding CL image is depicted in Figure 6b. These images suggest that

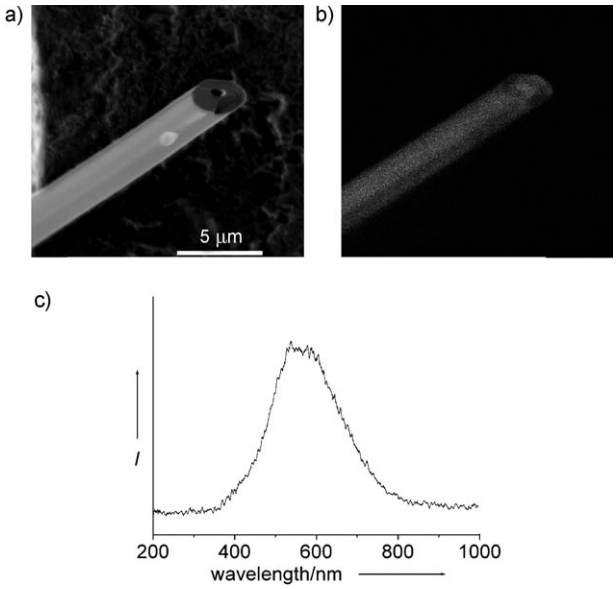

Figure 6. a) Thermal field emission SEM image of a hollow $In_2Ge_2O_7$ microtube; b) monochromatic CL image recorded at room temperature; c) CL spectrum of a hollow $In_2Ge_2O_7$ microtube.

the $In_2Ge_2O_7$ tube is optically uniform except for a small, bright dot within the pore region. The CL spectra collected from the various points over the $In_2Ge_2O_7$ tube show similar emissions (see Supporting Information). The CL spectrum (Figure 6c) recorded over the entire $In_2Ge_2O_7$ tube at room temperature shows a broad emission centered at around 560 nm. This luminescence may originate from the honeycomb sheets of $\{InO_6\}$ octahedra since the germanate groups most likely do not behave as luminescent centers in $In_2Ge_2O_7$, as was confirmed during a study on $Sc_2Ge_2O_7$ crystals with a very similar structure.[5]

In summary, monocrystalline, sub-micrometer $In_2Ge_2O_7$ tubes have been generated by carbon-assisted thermal co-

evaporation of In_2O_3 and GeO_2. Within an $In_2Ge_2O_7$ tube, the InO_6 octahedra laminae are parallel to the [100] preferential growth axis. The tube generation has been discussed from both thermodynamic and kinetic points of view. It is notable that the diameter of these $In_2Ge_2O_7$ tubes is similar to the wavelength and mean free path of photons.[19–22] Therefore, these novel tubular structures may find interesting potential applications as waveguides or microlasers.

Experimental Section

The indium germanate tubes were synthesized by a vapor transport and condensation process. A quartz crucible containing a ground mixture of In_2O_3 (1.11 g), GeO_2 (0.84 g), and activated carbon (0.20 g) powders was placed in the center of a quartz tube within a tube furnace. The furnace was heated to 1000 °C at a rate of 20 K min^{-1}, kept at this temperature for 2 h, and then allowed to cool to room temperature. The whole process was carried out under a constant flow of pure Ar at a rate of 200 std cm^3 min^{-1}. A white product was collected from the inner wall of the quartz tube. The overall yield was around 10% based on the amount of In_2O_3. The product was characterized by powder XRD (RINT 2200) with $Cu_{K\alpha}$ radiation (λ = 1.5418 Å), scanning electron microscopy (SEM, JSM-6700F), and by means of a high-resolution transmission electron microscope (HRTEM; JEM-3000F) equipped with an energy-dispersive X-ray spectrometer (EDS). Cathodoluminescence (CL) spectra were collected at room temperature with a high-spatial-resolution CL system attached to a thermal field-emission scanning electron microscope (TFE-SEM, Hitachi S4200) performing at 5 kV and 1.2 nA.

Received: August 12, 2005
Published online: November 29, 2005

Keywords: crystal growth · germanium · indium · nanotubes · semiconductors

[1] S. Iijima, *Nature* **1991**, *354*, 56–58.
[2] a) N. G. Chopra, R. J. Luyken, K. Cherrey, V. H. Crespi, M. L. Cohen, S. G. Louie, A. Zettl, *Science* **1995**, *269*, 966–967; b) K. Suenaga, C. Colliex, N. Demoncy, A. Loiseau, H. Pascard, F. Willaime, *Science* **1997**, *278*, 653–655; c) Y. Feldman, E. Wasserman, D. J. Srolovitz, R. Tenne, *Science* **1995**, *267*, 222–225; d) R. Tenne, *Angew. Chem.* **2003**, *115*, 5280–5289; *Angew. Chem. Int. Ed.* **2003**, *42*, 5124–5132; e) J. M. Macak, H. Tsuchiya, P. Schmuki, *Angew. Chem.* **2005**, *117*, 2136–2139; *Angew. Chem. Int. Ed.* **2005**, *44*, 2100–2102; f) Y. Q. Zhu, T. Sekine, K. S. Brigatti, S. Firth, R. Tenne, R. Rosentsveig, H. W. Kroto, D. R. W. Walton, *J. Am. Chem. Soc.* **2003**, *125*, 1329–1333; g) U. K. Gautam, S. R. C. Vivekchand, A. Govindaraj, G. U. Kulkarni, N. R. Selvi, C. N. R. Rao, *J. Am. Chem. Soc.* **2005**, *127*, 3658–3659; h) M. Nath, C. N. R. Rao, *Angew. Chem.* **2002**, *114*, 3601–3604; *Angew. Chem. Int. Ed.* **2002**, *41*, 3451–3454; i) H. A. Therese, F. Rocker, A. Reiber, J. X. Li, M. Stepputat, G. Glasser, U. Kolb, W. Tremel, *Angew. Chem.* **2005**, *117*, 267–270; *Angew. Chem. Int. Ed.* **2005**, *44*, 262–265; j) F. S. Cai, G. Y. Zhang, J. Chen, X. L. Gou, H. K. Liu, S. X. Dou, *Angew. Chem.* **2004**, *116*, 4308–4312; *Angew. Chem. Int. Ed.* **2004**, *43*, 4212–4216.
[3] a) P. M. Ajayan, O. Stephan, P. Redlich, C. Colliex, *Nature* **1995**, *375*, 564–567; b) K. J. C. van Bommel, A. Friggeri, S. Shinkai, *Angew. Chem.* **2003**, *115*, 1010–1030; *Angew. Chem. Int. Ed.* **2003**, *42*, 980–999; c) C. R. Martin, *Science* **1994**, *266*, 1961–1965; d) J. Goldberger, R. He, Y. Zhang, S. Lee, H. Yan, H. Choi, P. Yang, *Nature* **2003**, *422*, 599–602; e) J. Hu, Y. Bando, Z. Liu, J. Zhan, D. Golberg, T. Sekiguchi, *Angew. Chem.* **2004**, *116*, 65–68; *Angew. Chem. Int. Ed.* **2004**, *43*, 63–66; f) R. Ma, Y. Bando, D. Golberg, T. Sato, *Angew. Chem.* **2003**, *115*, 1880–1882; *Angew. Chem. Int. Ed.* **2003**, *42*, 1836–1838; g) A. R. Armstrong, J. Canales, P. G. Bruce, *Angew. Chem.* **2004**, *116*, 5007–5010; *Angew. Chem. Int. Ed.* **2004**, *43*, 4899–4902; h) X. Wang, J. Zhuang, J. Chen, K. Zhou, Y. Li, *Angew. Chem.* **2004**, *116*, 2051–2054; *Angew. Chem. Int. Ed.* **2004**, *43*, 2017–2020; i) Y. G. Sun, Y. N. Xia, *Adv. Mater.* **2004**, *16*, 264–268.
[4] a) T. E. Gier, X. Bu, P. Feng, G. D. Stucky, *Nature* **1998**, *395*, 154–157; b) D. Pitzschke, W. Bensch, *Angew. Chem.* **2003**, *115*, 4525–4528; *Angew. Chem. Int. Ed.* **2003**, *42*, 4389–4391; c) Y. Zhou, H. Zhu, Z. Chen, M. Chen, Y. Xu, H. Zhang, D. Zhao, *Angew. Chem.* **2001**, *113*, 2224–2226; *Angew. Chem. Int. Ed.* **2001**, *40*, 2166–2168; d) H. Li, M. Eddaoudi, O. M. Yaghi, *Angew. Chem.* **1999**, *111*, 682–685; *Angew. Chem. Int. Ed.* **1999**, *38*, 653–655; e) M. Avenier, G. Bagieu, R. Brissot, J. F. Cavaignac, J. Collot, D. H. Koang, D. Lebrun, F. Minot, A. Stutz, *Nucl. Phys. B* **1992**, *A28*, 496–499; f) M. J. Hogan, A. W. Brinkman, T. Hashemi, *Appl. Phys. Lett.* **1998**, *72*, 3077–3079.
[5] T. Gaewdang, J. P. Chaminade, P. Gravereau, A. Garcia, C. Fouassier, M. Pouchard, P. Hagenmuller, *Z. Anorg. Allg. Chem.* **1994**, *620*, 1965–1970.
[6] a) G. R. Patzke, F. Krumeich, R. Nesper, *Angew. Chem.* **2002**, *114*, 2554–2571; *Angew. Chem. Int. Ed.* **2002**, *41*, 2446–2461; b) X. Wang, Y. Li, *Angew. Chem.* **2002**, *114*, 4984–4987; *Angew. Chem. Int. Ed.* **2002**, *41*, 4790–4793; c) A. R. Armstrong, G. Armstrong, J. Canales, P. G. Bruce, *Angew. Chem.* **2004**, *116*, 2336–2338; *Angew. Chem. Int. Ed.* **2004**, *43*, 2286–2288; d) S. H. Yu, M. Antonietti, H. Cölfen, M. Giersig, *Angew. Chem.* **2002**, *114*, 2462–2466; *Angew. Chem. Int. Ed.* **2002**, *41*, 2356–2360.
[7] a) Z. R. Dai, Z. W. Pan, Z. L. Wang, *Adv. Funct. Mater.* **2003**, *13*, 9–24; b) R. Q. Zhang, Y. Lifshitz, S. T. Lee, *Adv. Mater.* **2003**, *15*, 635–640.
[8] a) Y. Wu, P. Yang, *J. Am. Chem. Soc.* **2001**, *123*, 3165–3166; b) J. Zhan, Y. Bando, J. Hu, T. Sekiguchi, D. Golberg, *Adv. Mater.* **2005**, *17*, 225–230; c) C. N. R. Rao, F. L. Deepak, G. Gundiah, A. Govindaraj, *Prog. Solid State Chem.* **2003**, *31*, 5–147.
[9] R. D. Shannon, A. W. Sleight, *Inorg. Chem.* **1968**, *7*, 1649–1651.
[10] R. D. Shannon, C. T. Prewitt, *J. Solid State Chem.* **1970**, *2*, 199–202.
[11] B. Gates, B. Mayers, A. Grossman, Y. N. Xia, *Adv. Mater.* **2002**, *14*, 1749–1752.
[12] H. K. Edwards, P. A. Salyer, M. J. Roe, G. S. Walker, P. D. Brown, D. H. Gregory, *Angew. Chem.* **2005**, *117*, 3621–3624; *Angew. Chem. Int. Ed.* **2005**, *44*, 3555–3558.
[13] J. Liu, Q. Li, T. Wang, D. Yu, Y. Li, *Angew. Chem.* **2004**, *116*, 5158–5162; *Angew. Chem. Int. Ed.* **2004**, *43*, 5048–5052.
[14] J. Yang, Y. C. Liu, H. M. Lin, C. C. Chen, *Adv. Mater.* **2004**, *16*, 713–716.
[15] Q. Wu, Z. Hu, X. Wang, Y. Lu, X. Chen, H. Xu, Y. Chen, *J. Am. Chem. Soc.* **2003**, *125*, 10176–10177.
[16] J. Zhan, Y. Bando, J. Hu, D. Golberg, *Inorg. Chem.* **2004**, *43*, 2462–2464.
[17] J. Hu, Y. Bando, J. Zhan, F. Xu, T. Sekiguchi, D. Golberg, *Adv. Mater.* **2004**, *16*, 1464–1468.
[18] E. P. A. M. Bakkers, M. A. Verheijen, *J. Am. Chem. Soc.* **2003**, *125*, 3440–3441.
[19] M. Law, D. J. Sirbuly, J. C. Johnson, J. Goldberger, R. J. Saykally, P. Yang, *Science* **2004**, *305*, 1269–1273.
[20] L. M. Tong, R. R. Gattass, J. B. Ashcom, S. L. He, J. Y. Lou, M. Y. Shen, I. Maxwell, E. Mazur, *Nature* **2003**, *426*, 816–819.
[21] R. Yang, G. Chen, *Nano Lett.* **2005**, *5*, 1111–1115.
[22] J. S. Foresi, P. R. Villeneuve, J. Ferrera, E. R. Thoen, G. Steinmeyer, S. Fan, J. D. Joannopoulos, L. C. Kimerling, H. I. Smith, E. P. Ippen, *Nature* **1997**, *390*, 143–145.

